




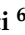




## Article

# Metabolic Stability of Eight Airborne OrganoPhosphate Flame Retardants (OPFRs) in Human Liver, Skin Microsomes and Human Hepatocytes

Stefano Di Bona <sup>1,†</sup>, Emanuele Artino <sup>2,†</sup>, Francesca Buiarelli <sup>3</sup>, Patrizia Di Filippo <sup>3,4</sup>, Roberta Galarini <sup>5</sup>, Stefano Lorenzetti <sup>6</sup>, Franco Lucarelli <sup>7</sup>, Gabriele Cruciani <sup>2</sup> and Laura Goracci <sup>2,\*</sup>

<sup>1</sup> Molecular Horizon s.r.l, 06084 Bettona, Italy; stefano.dibona@molhorizon.it

<sup>2</sup> Department of Chemistry, Biology and Biotechnology, University of Perugia, 06123 Perugia, Italy; emanuele.artino@studenti.unipg.it (E.A.); gabriele.cruciani@unipg.it (G.C.)

<sup>3</sup> Department of Chemistry, Sapienza University of Rome, 00185 Rome, Italy; francesca.buiarelli@uniroma1.it (F.B.); p.difilippo@inail.it (P.D.F.)

<sup>4</sup> Italian Workers' Compensation Authority (INAIL)—DIT, 00143 Rome, Italy

<sup>5</sup> Istituto Zooprofilattico Sperimentale dell'Umbria e delle Marche "Togo Rosati", 06126 Perugia, Italy; r.galarini@izsum.it

<sup>6</sup> Department of Food Safety, Nutrition and Veterinary Public Health, Istituto Superiore di Sanità, 00161 Rome, Italy; stefano.lorenzetti@iss.it

<sup>7</sup> Department of Physics and Astronomy and INFN, University of Florence, 50019 Sesto Fiorentino, Italy; lucarelli@fi.infn.it

\* Correspondence: laura.goracci@unipg.it; Tel.: +39-0755855632

† These authors contributed equally to this work.

**Abstract:** The waste of electrical and electronic equipment (WEEE) is generally considered a secondary raw material for the recovery of valuable components. However, emerging issues regarding the impact of suspended particles arising from WEEE recycling operations are a concern. It was recently demonstrated that samples from three different WEEE plants were rich in organophosphate flame retardants (OPFRs). Since exposure to a xenobiotic can lead to its biotransformation through human metabolism routes, in the present study, the metabolism of eight OPFRs of interest in our sampling campaign (triphenyl phosphate (TPhP), tri-*m*-tolyl phosphate (TMTP), ethylhexyl diphenyl phosphate (EHDPHP), tributoxylethyl phosphate (TBOEP), diphenyl phosphate (DPhP), trichloroethyl phosphate (TCEP), tris(1,3-dichloropropan-2-yl) phosphate (TDCIPP) and bisphenol A bis(diphenyl phosphate) (BDP)) was investigated. Their metabolism was studied at different time points in three matrices: human liver microsomes, human hepatocytes and human skin microsomes. This study, which was run using a common experimental setting, allowed easy comparison of results for each OPFR of interest, and a comparison with other data in the literature was performed. In particular, a number of metabolites not previously described were detected, and for the first time, it was shown that TPhP could be metabolized in human skin microsomes.

**Keywords:** WEEE; OPFR; metabolism; HLM; human hepatocytes; HSM



**Citation:** Di Bona, S.; Artino, E.; Buiarelli, F.; Di Filippo, P.; Galarini, R.; Lorenzetti, S.; Lucarelli, F.; Cruciani, G.; Goracci, L. Metabolic Stability of Eight Airborne OrganoPhosphate Flame Retardants (OPFRs) in Human Liver, Skin Microsomes and Human Hepatocytes. *Separations* **2023**, *10*, 548. <https://doi.org/10.3390/separations10110548>

Academic Editor: Victoria Samanidou

Received: 9 October 2023

Revised: 23 October 2023

Accepted: 23 October 2023

Published: 25 October 2023



**Copyright:** © 2023 by the authors. Licensee MDPI, Basel, Switzerland. This article is an open access article distributed under the terms and conditions of the Creative Commons Attribution (CC BY) license (<https://creativecommons.org/licenses/by/4.0/>).

## 1. Introduction

Since polybrominated diphenyl ester (PBDE) flame retardants were listed by the Stockholm Convention on Persistent Organic Pollutants for their environmental persistence and toxicity in 2009 and 2017 [1,2], organophosphate flame retardants (OPFRs) have found considerable use in the production of plasticizers, textiles, furniture, coatings, polyvinylchloride (PVC) plastics and polyurethane foams [3], leading to an increase in their production. Therefore, the global use of OPFRs increased a lot in recent years, including from 0.5 million tons in 2011 to 0.68 million in 2015 [4] and 2.39 million in 2019 [5], with a global annual increase of 2.7% estimated in the period 2019–2025 [5]. Despite their use as

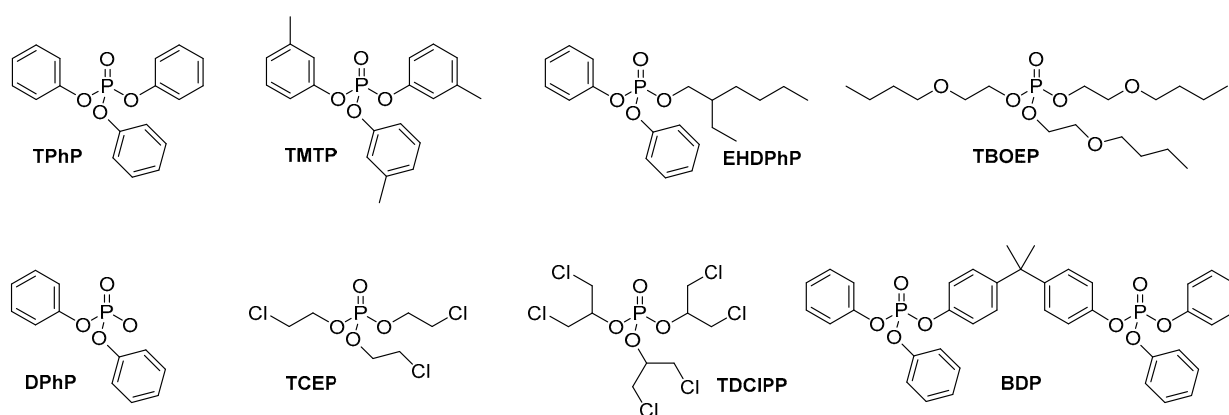
“safe alternatives” of PDBEs, several papers have been recently published showing that OPFRs have a high persistence and an easy diffusion in a series of environmental matrices such as soil [6], sediments [3], mud [3], dust [1,7–9], air [1], particulate [1], and waters such as oceans [10], rivers [11] and drinking waters [11,12]. As has previously occurred for PBDEs, the broad presence in the environment of OPFRs, such as organophosphate esters (OPEs), is now raising serious concerns about their safety; indeed, OPFRs are in direct contact with main human exposure pathways (inhalation, ingestion and skin absorption) [1] and they can cause adverse effects on human health. In recent studies, neurotoxicity effects have been observed in *in vitro* tests [13,14]. Moreover, exposition to OPFRs and their metabolites has been associated with the formation or progression of cancer of various origins such as prostate [15], gastrointestinal tract [16], breast [17], thyroid [18], as well as with thyroid hormones [19,20] and estrogen alteration [21]. Finally, toxic effects on keratinocytes were also observed [22].

OPFRs can undergo biotransformation, and their metabolites can also induce toxicity and adverse events due to bioaccumulation. Indeed, OPFRs, like general xenobiotics, can, in principle, be metabolized and eliminated through urine, bile, feces and by minor routes such as exhalation and sweat. Many compounds can reach toxic levels with dangerous health effects without effective detoxification and subsequent excretion [23]. To evaluate the safety of xenobiotics, metabolic stability assays are commonly performed to predict pharmacokinetics in humans [24]. Cytochrome P450-dependent monooxygenases (P450s) represent the primary enzyme system that induces the oxidative metabolism of xenobiotics. In particular, the liver, lung and skin microsomal P450s play a key role in converting lipophilic xenobiotics, including drugs, insecticides, carcinogens, food additives and environmental pollutants, to more polar compounds that are easier to excrete [25]. Several studies have demonstrated that OPFR metabolites, especially diester and hydroxylated forms, possess an even higher toxicity profile than their respective parent compounds [22]. In the case of environmental contaminants, exposure can be difficult to control, and *in vitro* studies aiming at extrapolating metabolic pathways can also be extremely useful for the generation of pharmacokinetic models to evaluate the safety of xenobiotics [24].

In the context of a research project to evaluate the environmental and health impact of organic emerging pollutants, we recently published a preliminary investigation on waste electrical and electronic equipment (WEEE) plants’ airborne particulate matter (PM) composition [26]. Among the classes of compounds investigated, OPEs were the major organic constituents, especially in the coarse fraction of PM. In this work, the metabolic stability studies of eight airborne OPFRs (Figure 1) identified in air particulate samples of waste electrical and electronic equipment (WEEE) plants were carried out [26,27]. In particular, liver metabolism was evaluated in human liver microsomes (HLM), which provide information on phase I biotransformations, and in human hepatocytes (HuHep), in which phase II metabolic reactions also occur. In addition to considering another mechanism of environmental exposure, metabolic stability in human skin microsomes (HSMs) was also evaluated. HSMs contain relevant enzymes that play a role in the metabolism of OPFR esters, such as P450s or, in particular, carboxylesterase [28]. The eight selected OPFRs were triphenyl phosphate (TPhP), tri-*m*-tolyl phosphate (TMTP), ethylhexyl diphenyl phosphate (EHDPHP), tributoxyethyl phosphate (TBOEP), diphenyl phosphate (DPhP), trichloroethyl phosphate (TCEP), Tris(1,3-dichloropropan-2-yl) phosphate (TDCIPP) and bisphenol A bis(diphenyl phosphate) (BDP) (Figure 1).

In the literature, previous studies have described the metabolism of TPhP, EHDPHP, TBOEP, TCEP and TDCIPP. For instance, one of the pioneering *in vitro* studies on the metabolism of OPFRs was published by Van den Eede et al. [29]. In that paper, TPhP, TBOEP, TCEP, tris(1-chloro-2-propyl) phosphate (TCIPP), and TDCPP were individually investigated for their metabolism in HLM and human liver S9 fractions after 1 h of incubation. Thus, Van den Eede et al. [29] proved that it was possible to detect a wide array of metabolites mainly due to oxidative metabolism, with TCEP associated with the lowest number of detected metabolites. In addition, a few phase II metabolites were also observed

for almost all the studied OPFRs. However, it is noteworthy that different matrices (e.g., HLM, S9 or HuHep) and experimental conditions (e.g., incubation time) were used in the literature [29–32]. In addition, at the time of writing, we are not aware of studies on human skin microsomes for these compounds, and, to the best of our knowledge, the metabolism of TMTP, DPhP and BDP has not been previously investigated in human matrices. Finally, in our study, we decided to apply a time-course approach, to monitor the formation of metabolites with time. Since a time-course study generated a larger amount of data compared to the traditional one-incubation-time approach to reduce the time needed for data analysis, the Mass-MetaSite software v1.0 [33] connected to the ONIRO platform [34,35] was used for the first time for the analysis of OPFRs. Our results are discussed and compared with previous published studies.



**Figure 1.** Chemical structures of OPFRs studied in this paper.

## 2. Materials and Methods

### 2.1. Chemicals and Reagents

Pooled human liver microsomes (HLM,  $n = 50$  mixed genders) and pooled human cryopreserved hepatocytes (HuHep,  $n = 10$  mixed gender) were purchased from Thermo Fischer Scientific (Frederick, MD, USA) and from Lonza (Basel, Switzerland), respectively, and pooled human skin microsomes (HSM,  $n = 3$  female gender) were purchased from Biopredic International (Saint Grégoire, France). The standards for EHDPHP and BDP were purchased from LGC (Teddington, UK), and standards for TPhP, DPhP, TMTP, TDCIPP, TCEP, TBOEP, and reduced  $\beta$ -nicotinamide adenine dinucleotide 2'-phosphate (NADPH) were purchased from Merck Life Science (Milan, Italy). Potassium phosphate dibasic and potassium phosphate monobasic were purchased from Merck Life Science (Milan, Italy), while William's E Medium and CM4000 were purchased from Thermo Fischer Scientific (Frederick, MD, USA). Milli-Q water was produced with a Sartorius Arius Mini Ultrapure water system (Goettingen, Germany) and acetonitrile and methanol hypergrade were produced for LC-MS analysis, and ammonium acetate, formic acid, and DMSO were purchased from Merck Life Science (Milan, Italy). The Kinetex<sup>®</sup> 1.7  $\mu\text{m}$  XB-C18 100 Å, LC Column 100  $\times$  2.1 mm was purchased from Phenomenex (Torrance, CA, USA).

### 2.2. In Vitro Incubations

To investigate the formation of phase-I metabolites for the eight OPFRs, the reaction mixture containing 100 mM of phosphate buffer at pH 7.4, OPFRs (20  $\mu\text{M}$ , final concentration), and human liver microsomes or human skin microsomes (1 mg/mL for HLM and 0.2 mg/mL for HSM final concentration) were preincubated in a Themomixer Eppendorf at 37 °C and 800 rpm. The reaction was initiated by the addition of NADPH (1 mM final concentration), and an aliquot of the incubation solution was taken at seven time points (0, 5, 10, 15, 30, 60, 90 min). The reaction was quenched with ice-cold acetonitrile (4 °C with labetalol as internal standard (1  $\mu\text{M}$ ) in the ratio of incubation solution: acetonitrile at

1:3 *v/v*. In the case of HuHep, they were thawed in a 37 °C shaking water bath according to the manufacturer's specifications and resuspended in Williams E medium (WEM) to obtain  $1 \times 10^6$  cells/mL. Samples with OPFRs at 20  $\mu$ M were incubated at 37 °C, and aliquots of 50  $\mu$ L were collected at 0, 30, 60, 120 and 240 min.

Once collected in microsomes or hepatocytes, samples were vortexed, kept at 4 °C for 10 min and centrifuged at 14,000 rpm for 10 min at 4 °C. Finally, the supernatant was transferred to new tubes and dried with N<sub>2</sub> stream at 35 °C. The samples were reconstituted with H<sub>2</sub>O/CH<sub>3</sub>OH 1:1 *v/v*. Blanks and control samples were prepared similarly but in the absence of the investigated compounds or NADPH, respectively.

### 2.3. LC-QTOF Method

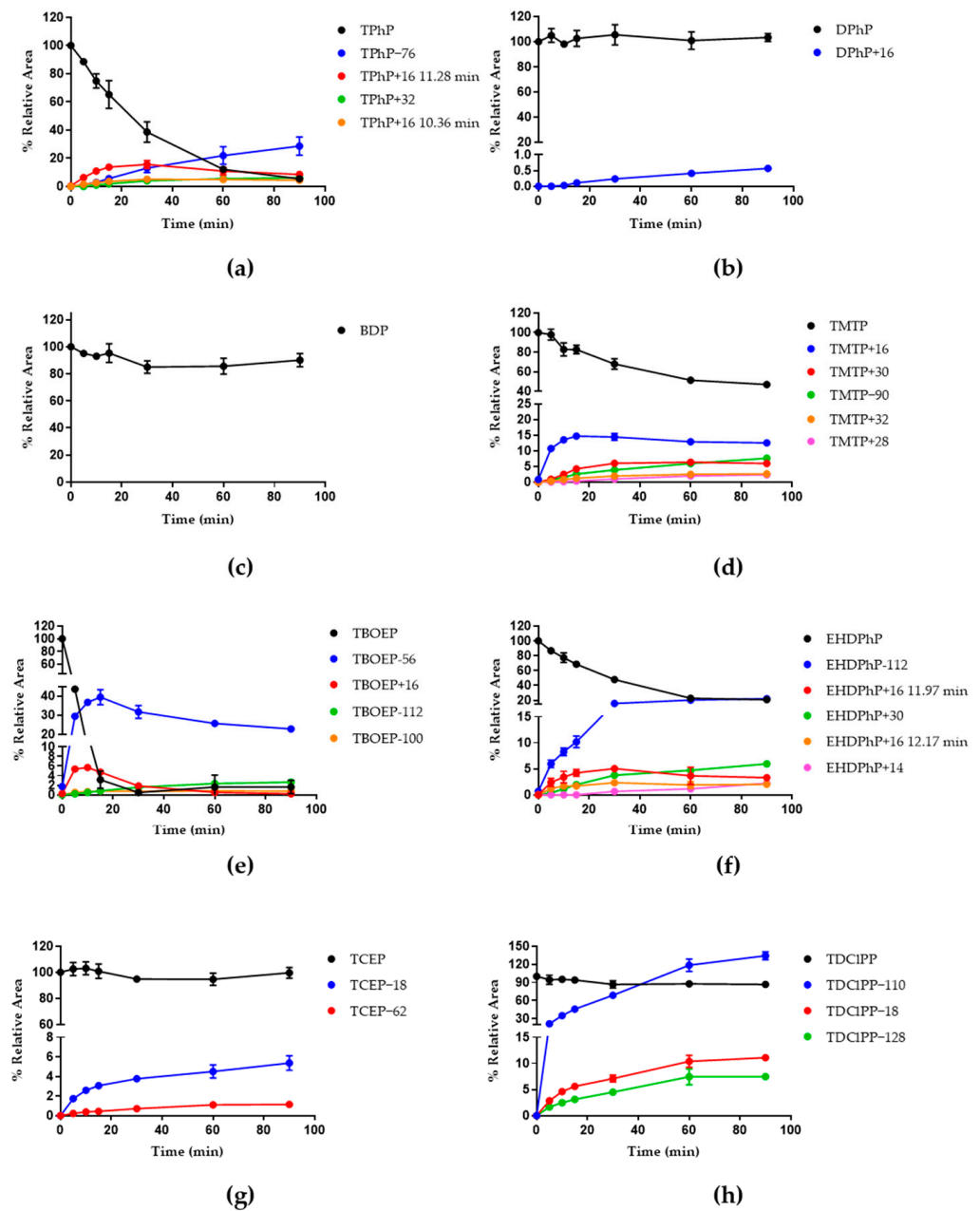
Samples were analyzed using liquid chromatography–mass spectrometry (LC–MS) in both a positive and negative mode using an HPLC 1290 series coupled to a 6540 UHD Accurate-Mass Q-TOF (Agilent Technologies, Santa Clara, CA, USA). The chromatographic separation of the metabolites formed was achieved using a Kinetex XB-C18 (100 mm  $\times$  2.1 mm  $\times$  1.7  $\mu$ m, Phenomenex), with 0.1% formic acid (A) and 0.1% formic acid in methanol (B) as mobile phases in the positive mode and 5 mM ammonium acetate (A) and 5 mM ammonium acetate in methanol (B) in the negative mode. In both the positive and negative modes, the same LC parameters exist. The gradient elution was as follows: 0.5% B at 0 min, a linear increase in B to 35%, from 0.5 to 6 min, a linear increase in B to 100%, from 6 to 14 min, followed by isocratic elution at 100% B from 14 to 16 min and a post-run of 4 min to re-equilibrate the column. The flow rate was 0.4 mL/min, the injection volume was 5  $\mu$ L and the column temperature was 40 °C.

The following ESI positive mode parameters were used: the MS and MS/MS scan range was set from *m/z* of 100 to 1700 amu, the MS and MS/MS scan rate was 3 spectra/s with an isolation width of 4 *m/z*, gas temperature at 300 °C, gas flow of 9 L/min, nebulizer pressure of 35 psig, sheath gas temperature at 320 °C, and a sheath gas flow of 9 L/min. The nozzle and capillary voltages were set to 0 V and 4000 V, respectively. For the ESI negative mode, the same settings were applied except for Nozzle and capillary voltages, which were set at 3500 and 500 V. The collision energy for the negative mode was set at 10 V.

## 3. Results and Discussion

### 3.1. Metabolism in HLM

In HLM, TPhP rapidly underwent biotransformation with a half-life time of 23.19 min (Figure 2a). In a previous study, Van den Eede et al. [29] identified phase I metabolites consisting of monohydroxylated forms (TPhP+16), diphenyl phosphate (TPhP–76), and a dihydroxylated form with hydroxyl groups linked to the same phenyl ring (TPhP+32). In our study, TPhP metabolism (Figure 2a) showed how two TPhP+16 metabolites were also identified as two isomers, resulting in them appearing chromatographically and adequately separated at retention times (R.T.) of 10.36 and 11.28 min. Moreover, our time-course experiments showed that TPhP+32 is likely to originate from the TPhP+16 metabolite at R.T. 11.28, as the latter decreased at 60 and 90 min. The single peak was identified as the dihydroxylated form of TPhP (TPhP+32) at R.T. 10.85 min and showed an MS/MS fragmentation pattern compatible with a dihydroxylation at the same phenyl ring (Figure 3a), although the exact position could not be elucidated. Finally, diphenyl phosphate (TPhP–76) was also clearly observed, and its formation with time seemed to be slower compared to the formation of hydroxylated forms. In comparison with the Van den Eede et al. study [29], we could not detect the second-generation metabolite TPhP–50, which originated from TPhP+16 due to the loss of a phenyl group. The absence of TPhP–50 can be explained by competition with the dihydroxylation reaction, and thus, this second-generation metabolite could be below the limit of detection (Supplementary Materials Table S1).

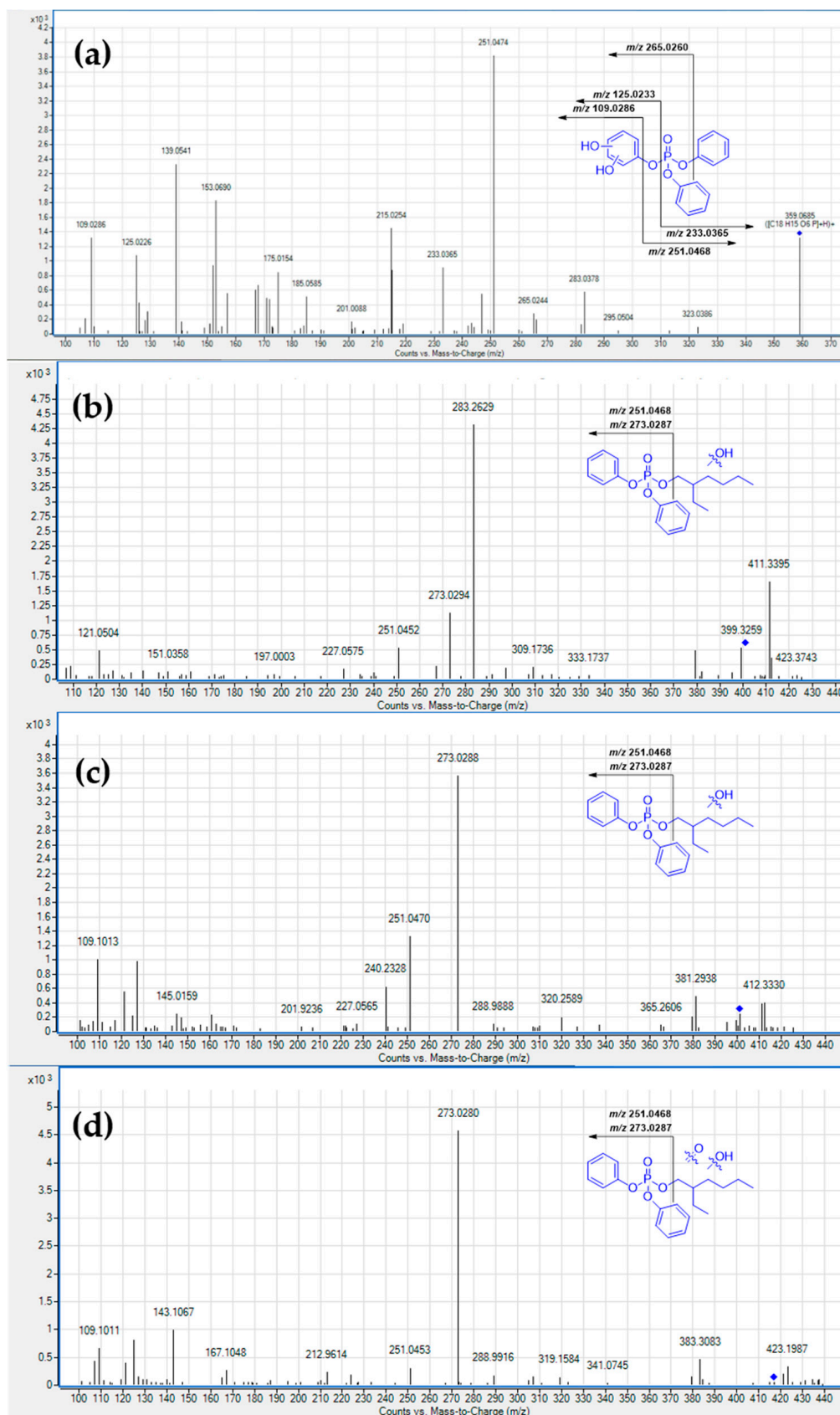


**Figure 2.** Metabolic profile in HLM for the eight substrates: TPhP (a), DPhP (b), BDP (c), TMTP (d), TBOEP (e), EHDPhP (f), TCEP (g) and TDCIPP (h). The observed behavior for substrate degradation is shown in black. The curves for metabolites are colored based on their maximum peak area value with the following order: blue > red > green > orange > pink > light blue > purple > yellow > grey.

Although the metabolism of TPhP has already been studied in various matrices, to the best of our knowledge, the main metabolite diphenyl phosphate DPhP has not been previously used as a substrate in metabolism studies. Nevertheless, acute and chronic exposure to DPhP led to high levels in the blood and other tissues, and multiomics analysis demonstrated a biological effect that was not observed when DPhP was generated as a metabolite of TPhP [30]. Therefore, we decided that DPhP deserved further investigation. When tested in HLM, DPhP showed higher metabolic stability (Figure 2b), with a single hydroxylated form of DPhP (DPhP+16) detected at R.T. 4.93 min (Supplementary Materials Table S2). Similarly, BDP was also characterized by high metabolic stability in HLM, and in this case, the slight signal decrease was not associated with any potential metabolites both in the positive and negative modes. (Figure 2c) A previous study by Alves et al. [31]



on BDP in HLM and in the absence of NADPH revealed the formation of six metabolites, which were likely formed by hydrolytic enzymes (Supplementary Materials Table S3). However, in our experimental conditions, those hydrolysis products were not detected either through Mass-MetaSite or manually. In HLM, TMTP resulted in a clearance of 50% at 90 min of incubation time, with the detection of five metabolites. (Figure 2d) Specifically, the metabolite that formed faster corresponded to a monohydroxylated metabolite (TMTP+16). In addition, other minor metabolites were detected, such as the dihydroxylated metabolite (TMTP+32), the dialdehyde metabolite (TMTP+28), oxidation to carboxyl acid (TMTP+30) and the O-dearylation of TMTP (TMTP−90). It is noteworthy that TMTP, to the best of our knowledge, has not been studied before in HLM (Supplementary Materials Table S4). Concerning TBOEP, this OPFR was rapidly metabolized in HLM, with complete clearance of the substrate after 30 min of incubation time. Among the eight substrates investigated, TBOEP was the most metabolically unstable one in HLM in our experimental conditions. In particular, a considerable phase I metabolism was observed (Figure 2e) with four metabolites identified. Previous studies on TBOEP in HLM led to the detection of different phase I metabolites correlated with dealkylation to give dibutoxyethyl phosphate (TBOEP−100), dibutoxyethyl ethylhydroxy phosphate (TBOEP−56) and two isomers obtained from the hydroxylation of the alkyl-ether chain which provided TBOEP+16. Metabolites of the second generation have been reported in HLM in *in vitro* studies such as the oxidative pathway for TBOEP−56 to obtain an aldehyde (TBEP−58), the carboxylic acid (TBOEP−42), the hydroxylation of TBOEP−100 (TBOEP−84) or its debutylation (TBOEP−156), the hydroxylation of TBOEP−56 (TBOEP−40) or the oxidative pathway for TBOEP−16 to obtain an aldehyde (TBOEP+14) a carboxylic acid (TBEP+30) or the simple secondary hydroxylation to obtain TBOEP+32 [29,32]. In our study, four metabolites were observed. Three of them were among those previously described in the literature [29,32]: a monohydroxylated TBOEP (TBOEP+16) at R.T. 11.39 min, the mono-debutylation (TBOEP−56) and the mono-debutoxyethylation (TBOEP−100) of the substrate, respectively. The position of the hydroxyl group is not determinable from MS/MS spectra due to the absence of characteristic fragments. Other metabolites reported in the literature have not been found, probably due to a lower concentration in samples. However, an additional metabolite which was not previously reported was observed in the positive ion mode, and this was identified as the di-debutylation of TBOEP to provide butoxyethyl di ethylhydroxy phosphate (TBOEP−112) (Supplementary Materials Table S5). In Figure 2f, the metabolic profile with time for EHDPHP is shown. This compound was metabolized with the complete disappearance of the substrate at 90 min. Although our analysis was qualitative, the most intense signal was associated with the diphenyl phosphate (EHDPHP−112), followed by two hydroxylated species of EHDPHP (EHDPHP+16) at R.T. 11.97 and 12.17 min. Moreover, other detected metabolites included the aldehyde or ketone form of EHDPHP (EHDPHP+14) and an additional metabolite named EHDPHP+30. A closer inspection of the MS/MS spectra of two hydroxylated metabolites EHDPHP+16 revealed that, in both cases, hydroxylation occurred at the alkyl chain moiety and not at the phenyl rings; indeed, fragments with  $m/z$  273.0232 and 251.0452 in the MS/MS spectra of EHDPHP+16 at R.T. 11.97 min (Figure 3b) and those with  $m/z$  273.0288 and 251.0450 in the MS/MS spectra of EDPhP+16 at R.T. 12.17 min (Figure 3c) can be associated with sodium adducts and the protonated diphenyl phosphate fragment. For EHDPHP+30, MS/MS spectra are in agreement with further oxidation at the alkyl chain level (Figure 3d) (Supplementary Materials Table S6). In Figure 3, additional fragments whose masses were heavier than the selected parent ion in MS/MS spectra, as well as some additional detected fragments, were likely due to co-eluting compounds that passed the parent ion isolation window (see Section 2).



**Figure 3.** MS/MS spectra of metabolites TPHP+32 (a), EHDPhP+16 at R.T. 11.97 min (b), EDPhP+16 at R.T. 12.17 min (c) and EHDPhP+30 (d) With characteristic fragments.

The metabolism of TCEP in HLM is summarized in Figure 2g. High metabolic stability in HLM without the clear disappearance of the substrate at different incubation times was observed. Nevertheless, two potential metabolites were detected from LC-MS analysis with low relative peak areas compared to the substrate. TCEP's metabolism in HLM was also studied by Van den Eede et al. [29], and the formation of two primary metabolites from the dealkylation of TCEP provided bis (2-chloroethyl) hydrogen phosphate (TCEP–62), while the oxidative dehalogenation gave 2-hydroxyethyl 2-chloroethyl hydrogen phosphate (TCEP–18) obtained from phase I metabolism. In our study, the detected metabolites TCEP–62 and TCEP–18 agreed with data from the literature (Supplementary Materials Table S7). Van den Eede et al. [29] also studied the metabolism of TDCIPP in HLM with the formation of four metabolites from the dealkylation of TDCIPP to the production of bis(1,3-dichloro-2-propyl) phosphate (TDCIPP–110), the oxidative dehalogenation of the substrate (TDCIPP–18) and relative metabolite bis(1,3-dichloro-2-propyl) phosphate (TDCIPP–128). TDCIPP–128 undergoes another oxidation of the hydroxyl group in the carboxyl group (TDCIPP–4). TDCIPP underwent degradation, decreasing by only 10% after 90 min (Figure 2h). The formation of three phase I metabolites obtained via dealkylation (TDCIPP–110), oxidative dehalogenation (TDCIPP–18) and TDCIPP–128 are in agreement with data from the literature (Supplementary Materials Table S8) [29].

### 3.2. HuHep Incubation

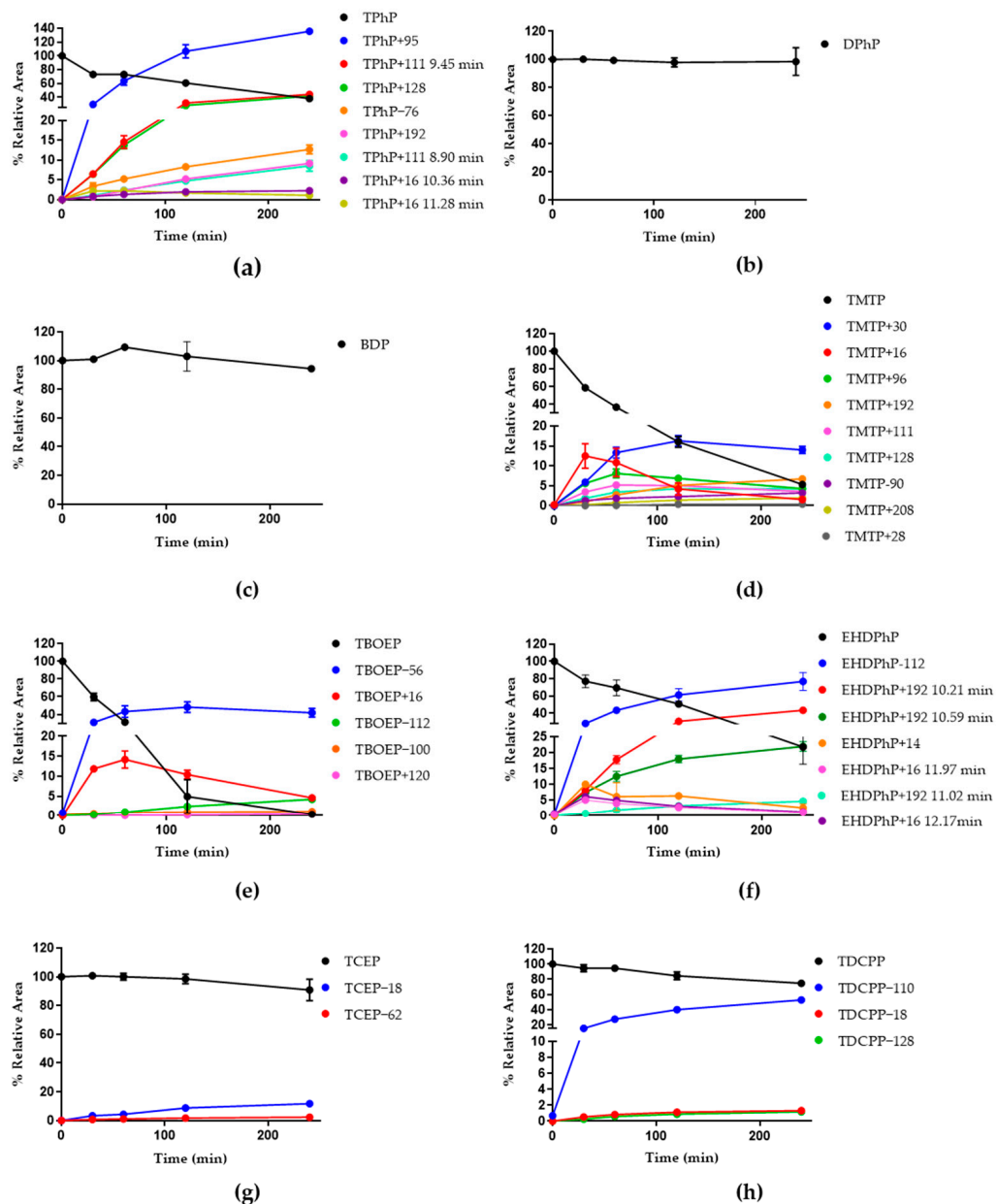
For TPhP, phase I metabolites observed upon incubation in HuHep were the same as those observed in HLM, with the exception of TPhP+32, which was not detected (Figure 4a). Concerning phase II metabolites, glucuronide and sulfate conjugates of monohydroxylated (TPhP+192, TPhP+95, respectively), and two sulfate conjugates of dihydroxylated TPhP were detected (TPhP+111 at R.T. 8.90 and 9.45 min). The obtained data were partially in line with Van der Eede et al. [29] because glucuronide conjugates TPhP+192, sulfate conjugates TPhP+95, and the two TPhP+111 metabolites were already detected, but the metabolite in our study, the glucuronide conjugates of dihydroxylated TPhP metabolite (TPhP+208), was not observed. However, in our experimental conditions, another sulfate with conjugate form (TPhP+128) was detected, which was formed from a trihydroxylated TPhP.

MS/MS spectra acquired in the negative mode and associated with the peaks identified as TPhP+111 at R.T. 8.90 and 9.45 min (Figure 5a,b, respectively) indicated that the dihydroxylation occurs on the same phenyl ring for the metabolite at 9.45 min and on two different phenyl rings for the metabolite at 8.90 min. Informative fragments were  $m/z$  249.0318 or 265.0262. The fragment at  $m/z$  249.0318 is also present in MS/MS spectra of metabolite TPhP+128 (Figure 5c), indicating the presence of two hydroxyl groups on a phenyl ring and the third hydroxylation is on another phenyl ring (Supplementary Materials Table S1).

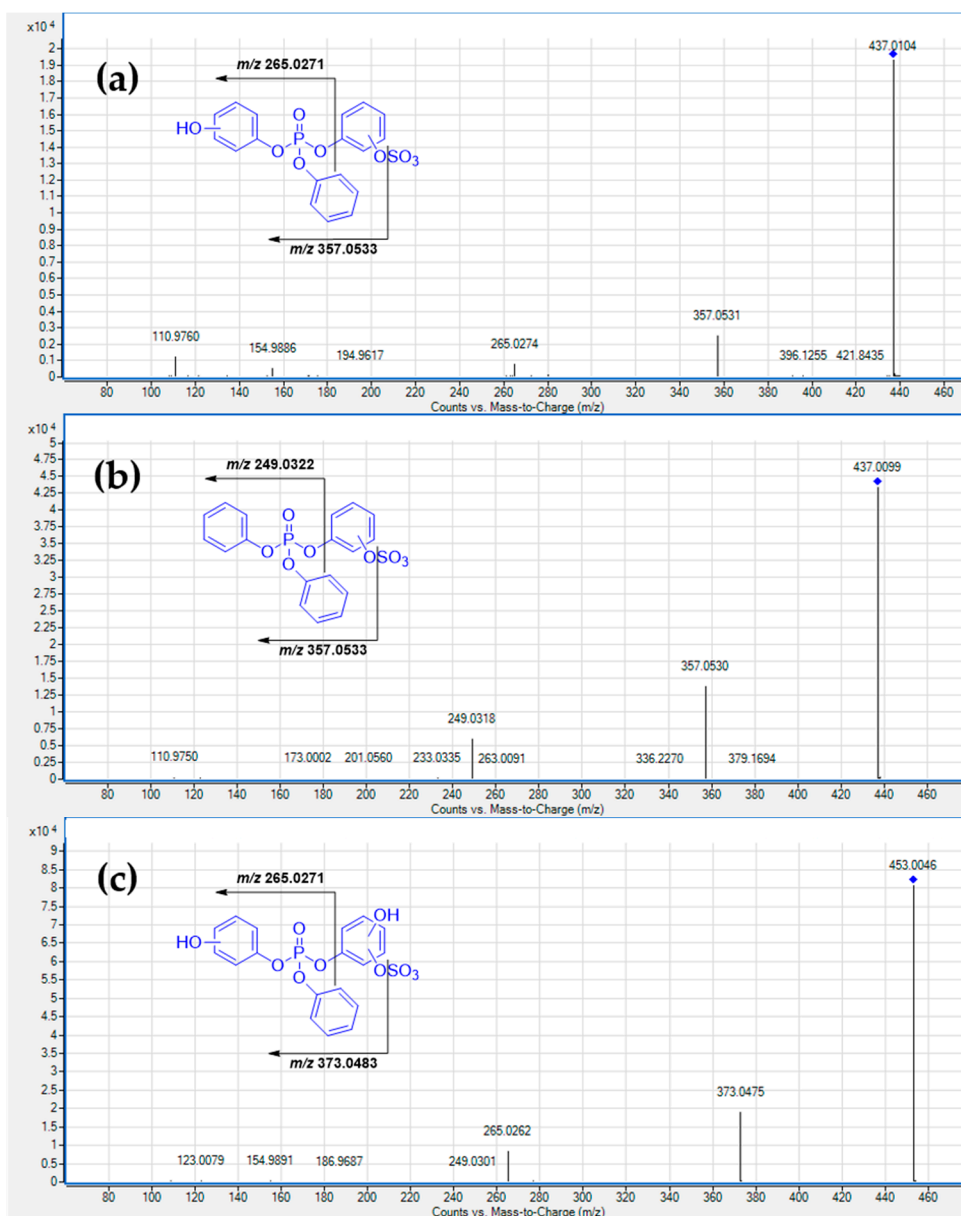
DPhP showed high metabolic stability in the metabolic studies in HuHep, with no metabolites detected (Figure 4b, Supplementary Materials Table S2). BDP resulted in high stability as it did not exhibit any metabolite in HuHep, similar to what was described for HLM incubation (Figure 4c and Supplementary Materials Table S3). Contrarily, in HuHep, TMTP underwent considerable phase I and phase II metabolism. A complete disappearance of the substrate after 240 min was observed, with the detection of 10 metabolites (Figure 4d). Specifically, for phase I metabolism, the formation of a single mono-hydroxylated metabolite (TMTP+16) and TMTP+16 also resulted in an intermediate metabolite leading to the formation of the carboxyl form (TMTP+30) to the dearylated species (TMTP–90) or to an undetected metabolite such as dihydroxylated tri-*m*-tolyl phosphate which is rapidly converted to the dialdehyde metabolite (TMTP+28). In addition to phase I metabolites, five phase II metabolites were detected as follows: indeed, the conjugations of glucuronic acid to monohydroxylated (TMTP+192) and dihydroxylated TMTP (TMTP+208) were observed, as well as the conjugation of a sulfate group to hydroxylated forms of TMTP (TMTP+96 for mono-, TMTP+111 for di- and TMTP+128 for tri-). The TMTP+128 metabolite suggested the presence of trihydroxylated metabolite TMTP+48, but we could not detect it in LC-



MS analysis both in the positive and negative mode (Supplementary Materials Table S4). Concerning TBOEP, this compound was rapidly metabolized, with the detection of the same phase I metabolite identified in HLM (Figure 4e). In addition, a phase II metabolite was identified as a glucuronide conjugate of TBOEP–56 (TBOEP+120). Unlike aryl-OPFRs, where the main phase II metabolites resulted in the conjugation of the sulfate moiety to a hydroxyl group on a phenyl ring, TBOEP, which lacks aromatic groups, was more prone toward the conjugation of glucuronic acid (Supplementary Materials Table S5).



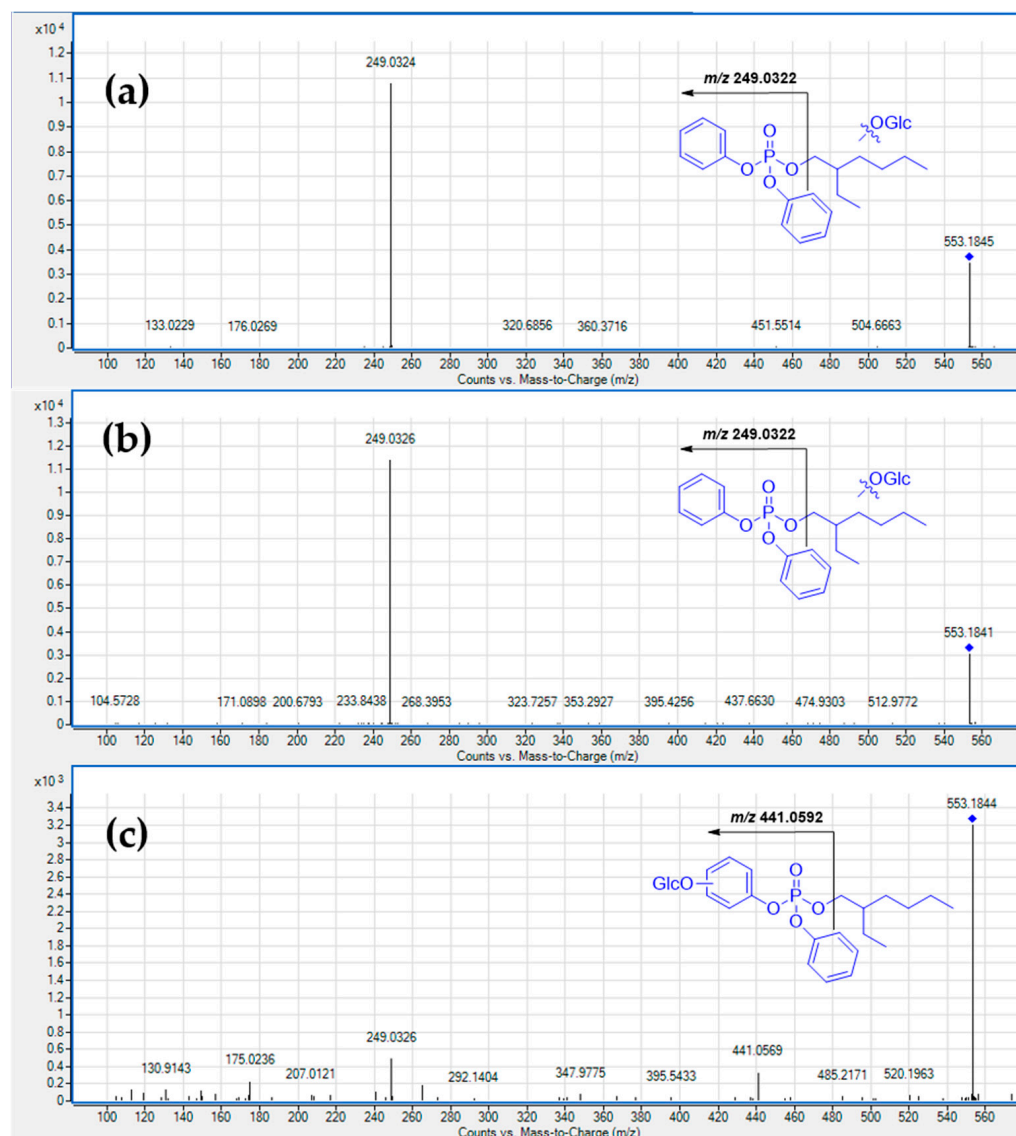
**Figure 4.** Kinetic curves of the 8 substrates (black curves) and their metabolites in HuHep incubation experiments for TPhP (a), DPhP (b), BDP (c), TMTP (d), TBOEP (e), EHDPhP (f), TCEP (g) and TDCIPP (h). The metabolite curves were painted in different colors in function of their relative abundance from the most abundance to the lowest in the following order: blue, red, green, orange, pink, light blue, purple, yellow and grey.



**Figure 5.** MS/MS Spectra of metabolite TPhP+111 at R.T. 8.90 min (a), at 9.45 min (b) and for metabolite TPhP+128 (c) with characteristic fragments.

Figure 4f shows the results of the metabolism study in HuHep for EHDPhP. The phase I metabolites identified were EHDPhP–112 and two EHDPhP+16s eluting at R.T. 11.97 and 12.17 min and EHDPhP+14. Compared to the metabolites detected upon incubation in HLM, the same metabolites were observed with the exception of EHDPhP+30, which is absent in HuHep incubation samples. Moreover, three-phase II metabolites were detected and resulted in three glucuronide conjugation products of EHDPhP (EHDPhP+192 at R.T. 10.21, 10.59 and 11.02 min). The MS/MS spectra of three EHDPhP+192 metabolites provided hints on the position of the glucuronide group (Figure 6). In particular,  $[M-H]^-$  species for the EHDPhP+192 metabolite at R.T. 11.02 min (Figure 6c) was characterized by a fragment at  $m/z$  441.0592 relative to neutral loss of the ethylhexyl chain. The presence of this fragment suggests that the glucuronide conjugation occurs on a phenyl moiety. For the other EHDPhP+192 metabolites at R.T. 10.21 min and R.T. 10.59 min, the fragment at  $m/z$  441.0592 was not observed in the corresponding MS/MS spectra (Figure 6a,b), suggesting that, in those cases, glucuronide conjugation occurs at different positions in the ethylhexyl chain (Supplementary Materials Table S6).

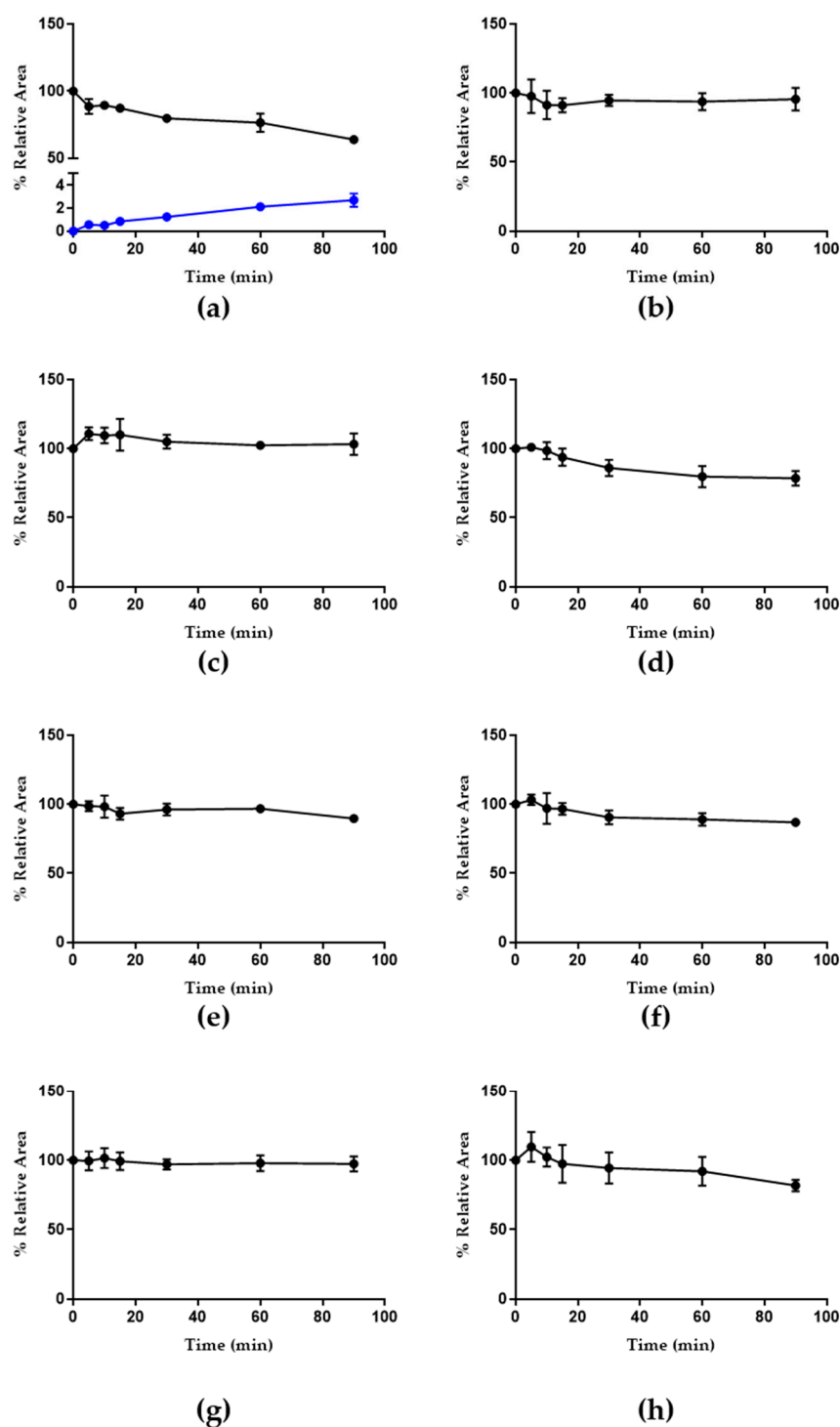
For TCEP incubation, the same metabolites (TCEP–18 and TCEP–62) formed in HLM were also observed upon incubation in HuHep (Figures 2g and 4g, respectively). In HuHep, a higher relative peak area for these metabolites was detected, and phase II metabolites were not observed (Supplementary Materials Table S7). These results are in agreement with Van den Eede et al. data [29], where the formation of phase II metabolites was similarly not observed. TDCIPP incubation provides the disappearance of 25% of the substrate at 240 min of incubation time with the formation of the same phase I metabolites already observed upon HLM incubation (Figure 4h). No phase II metabolites were detected either in the positive or negative mode (Supplementary Materials Table S8).



**Figure 6.** MS/MS spectra of metabolite EHDPhP+192 at R.T. 10.21 min (a), at R.T. 10.59 min (b) and for metabolite EHDPhP+192 at R.T. 11.02 min (c) with characteristic fragments.

### 3.3. HSM Incubation

In HSM, TPhP was less metabolized than in HLM, and the only metabolite detected was TPhP-76 (Figure 7a). This result indicates that human skin microsomes might also play a role in the metabolism of TPhP (Supplementary Materials Table S1).



**Figure 7.** Kinetic curves of the 8 substrates and their metabolites in HSM incubation experiments for TPhP (a), DPhP (b), BDP (c), TMTP (d), TBOEP (e), EHDPPhP (f), TCEP (g) and TDCIPP (h). The metabolite curve for TPhP–76 is painted in blue.

Differently from HLM data, in HSM, high metabolic stability was observed for all the other OPFRs investigated (Figure 7b–h).

The differences between HLM and HSM data suggest the major role of P450s on OPFR metabolism compared to esterases, considering the different distribution of these classes of enzymes in the two matrices [36].

#### 4. Conclusions

A systematic metabolism study for eight OPFRs identified in air particulate samples of waste electrical and electronic equipment (WEEE) recycling points was carried out in three human matrices (HLM, HuHep and HSM). In the case of metabolism data on human liver matrices (HLM and HuHep), TMTP metabolism was investigated for the first time, and a massive phase I and phase II metabolism was observed. Moreover, non-previously detected metabolites were identified for TPhP, such as two TPhP+16 isomers and a sulfation product from the trihydroxylated metabolite. In addition, other novel metabolites were detected in our study: for TBOEP, the formation of bis-debutylated metabolite was observed, while for EHDPHP, the metabolite with a carbonylic and hydroxyl function on ethylhexyl chain was detected.

BDP resulted in metabolic stability under the used experimental conditions both in HLM and HuHep. Therefore, hydrolysis products previously described for BDP in rat and bird liver microsomes [37] were not observed. Concerning DPhP, high metabolic stability was also observed in liver-related matrices, with only one metabolite observed in HLM. The absence of detectable metabolites in HuHep for DPhP suggested that the biological effects found by Selmi-Ruby et al. [30] are attributable to DPhP and not to potential metabolites.

In addition to human liver matrix data, metabolism in HSM for the selected OPFRs was reported for the first time. We found that the only OPFR undergoing a slight metabolism was TPhP with the formation of diphenyl phosphate, while the other OPFRs resulted metabolically stable in the used experimental conditions.

For halogenated OPFRs, the main metabolic pathway appeared to mainly involve diacylation and oxidative dehalogenation reactions. Thus, this behavior differs from the one observed for aryl- and alkyl-OPFRs, for which oxidation products are mostly observed. In particular, for alkyl-OPFRs, the formation of hydroxylated metabolites with soft spots located in the alkyl chains resulted in a common trend. However, for TBEOp, O-dealkylation reactions also occurred due to the presence of oxyethylene moieties in chains. Among all the OPFRs investigated, TBEOp was the least stable compound. Overall, the performed study contributes to increasing the knowledge of the metabolism of a series of OPFRs, including stability studies in skin matrices.

**Supplementary Materials:** The following supporting information can be downloaded at: <https://www.mdpi.com/article/10.3390/separations10110548/s1>: Table S1: LC-MS data for TPhP and its detected metabolites in HLM, HuHep and HSM; Table S2: LC-MS data for DPhP and its detected metabolites in HLM, HuHep and HSM; Table S3: LC-MS data for BDP and its detected metabolites in HLM, HuHep and HSM; Table S4: LC-MS data for TMTP and its detected metabolites in HLM, HuHep and HSM; Table S5: LC-MS data for TBEOp and its detected metabolites in HLM, HuHep and HSM; Table S6: LC-MS data for EHDPHP and its detected metabolites in HLM, HuHep and HSM; Table S7: LC-MS data for TCEP and its detected metabolites in HLM, HuHep and HSM; Table S8: LC-MS data for TDCIPP and its detected metabolites in HLM, HuHep and HSM.

**Author Contributions:** All authors contributed to the investigation. Conceptualization, G.C. and L.G.; methodology, S.D.B., L.G. and E.A.; LC-MS analysis, S.D.B. and E.A., Data interpretation, L.G., S.D.B. and E.A.; resources: F.B., R.G., F.L., S.L. and P.D.F., writing—original draft preparation, L.G., E.A. and S.D.B.; project administration, F.L. All authors have read and agreed to the published version of the manuscript.

**Funding:** This work was supported by the Italian Workers' Compensation Authority (INAIL), (grant number BRIC2019 ID13), Italy.

**Data Availability Statement:** All data generated or analyzed during this study are included in this published article and its Supplementary Materials file.

**Conflicts of Interest:** The authors declare no conflict of interest.



## References

1. Blum, A.; Behl, M.; Birnbaum, L.; Diamond, M.L.; Phillips, A.; Sipes, N.S.; Stapleton, H.M.; Venier, M. Organophosphate Ester Flame Retardants: Are They a Regrettable Substitution for Polybrominated Diphenyl Ethers? *Environ. Sci. Technol. Lett.* **2019**, *6*, 638–649. [[CrossRef](#)]
2. Sharkey, M.; Harrad, S.; Abdallah, M.A.; Drage, D.S.; Berresheim, H. Phasing-out of legacy brominated flame retardants: The UNEP Stockholm Convention and other legislative action worldwide. *Environ. Int.* **2020**, *144*, 106041. [[CrossRef](#)]
3. Wang, J.; Guo, Y.; Zhao, S.; Huang, R. A novel intumescent flame retardant imparts high flame retardancy to epoxy resin. *Polym. Adv. Technol.* **2019**, *31*, 932–940. [[CrossRef](#)]
4. Van Der Veen, I.; De Boer, J. Phosphorus flame retardants: Properties, production, environmental occurrence, toxicity and analysis. *Chemosphere* **2012**, *88*, 1119–1153. [[CrossRef](#)]
5. Azizi, S.; Hadi, M.; Naddafi, K.; Nabizadeh, R. Occurrence of organophosphorus esters in outdoor air fine particulate matter and comprehensive assessment of human exposure: A global systematic review. *Environ. Pollut.* **2023**, *318*, 120895. [[CrossRef](#)] [[PubMed](#)]
6. Zhang, Q.; Wang, Y.; Zhang, C.; Yao, Y.; Wang, L.; Sun, H. A review of organophosphate esters in soil: Implications for the potential source, transfer, and transformation mechanism. *Environ. Res.* **2022**, *204*, 112122. [[CrossRef](#)]
7. Chupeau, Z.; Bonvallot, N.; Mercier, F.; Bot, B.L.; Chevrier, C.; Glorennec, P. Organophosphorus Flame Retardants: A Global Review of Indoor Contamination and Human Exposure in Europe and Epidemiological Evidence. *Int. J. Environ. Res. Public Health* **2020**, *17*, 6713. [[CrossRef](#)] [[PubMed](#)]
8. Brits, M.; Brandsma, S.H.; Rohwer, E.R.; De Vos, J.; Weiss, J.M.; De Boer, J. Brominated and organophosphorus flame retardants in South African indoor dust and cat hair. *Environ. Pollut.* **2019**, *253*, 120–129. [[CrossRef](#)]
9. Li, W.; Wang, Y.; Kannan, K. Occurrence, distribution and human exposure to 20 organophosphate esters in air, soil, pine needles, river water, and dust samples collected around an airport in New York state, United States. *Environ. Int.* **2019**, *131*, 105054. [[CrossRef](#)]
10. Xie, Z.; Wang, P.; Wang, X.; Castro-Jiménez, J.; Kallenborn, R.; Liao, C.; Mi, W.; Lohmann, R.; Vila-Costa, M.; Dachs, J. Organophosphate ester pollution in the oceans. *Nat. Rev. Earth Environ.* **2022**, *3*, 309–322. [[CrossRef](#)]
11. Liang, C.; Mo, X.; Xie, J.; Wei, G.; Liu, L. Organophosphate tri-esters and di-esters in drinking water and surface water from the Pearl River Delta, South China: Implications for human exposure. *Environ. Pollut.* **2022**, *313*, 120150. [[CrossRef](#)] [[PubMed](#)]
12. Kim, U.; Kannan, K. Occurrence and Distribution of Organophosphate Flame Retardants/Plasticizers in Surface Waters, Tap Water, and Rainwater: Implications for Human Exposure. *Environ. Sci. Technol.* **2018**, *52*, 5625–5633. [[CrossRef](#)]
13. Bajard, L.; Melymuk, L.; Blaha, L. Prioritization of hazards of novel flame retardants using the mechanistic toxicology information from ToxCast and Adverse Outcome Pathways. *Environ. Sci. Eur.* **2019**, *31*, 14. [[CrossRef](#)]
14. Behl, M.; Hsieh, J.-H.; Shafer, T.J.; Mundy, W.R.; Rice, J.R.; Boyd, W.A.; Freedman, J.H.; Hunter, E.S.; Jarema, K.A.; Padilla, S.; et al. Neurotoxicology and Teratology Use of alternative assays to identify and prioritize organophosphorus flame retardants for potential developmental and neurotoxicity. *Neurotoxicol. Teratol.* **2015**, *52*, 181–193. [[CrossRef](#)]
15. Zhang, X.; Lu, Z.; Ren, X.; Chen, X.; Zhou, X.; Zhou, X.; Zhang, T.; Liu, Y.; Wang, S.; Qin, C. Ecotoxicology and Environmental Safety Genetic comprehension of organophosphate flame retardants, an emerging threat to prostate cancer. *Ecotoxicol. Environ. Saf.* **2021**, *223*, 112589. [[CrossRef](#)]
16. Li, Y.; Fu, Y.; Hu, K.; Zhang, Y.; Chen, J.; Zhang, S.; Zhang, B.; Liu, Y. Positive correlation between human exposure to organophosphate esters and gastrointestinal cancer in patients from Wuhan, China. *Ecotoxicol. Environ. Saf.* **2020**, *196*, 110548. [[CrossRef](#)] [[PubMed](#)]
17. Böckers, M.; Paul, N.W.; Thomas, E. Organophosphate ester tri-o-cresyl phosphate interacts with estrogen receptor  $\alpha$  in MCF-7 breast cancer cells promoting cancer growth. *Toxicol. Appl. Pharmacol.* **2020**, *395*, 114977. [[CrossRef](#)]
18. Liu, M.; Li, A.; Meng, L.; Zhang, G.; Guan, X.; Zhu, J.; Li, Y.; Zhang, Q.; Jiang, G. Exposure to Novel Brominated Flame Retardants and Organophosphate Esters and Associations with Thyroid Cancer Risk: A Case—Control Study in Eastern China. *Environ. Sci. Technol.* **2022**, *56*, 17825–17835. [[CrossRef](#)]
19. Hu, L.; Zhou, B.; Li, Y.; Song, L.; Wang, J.; Yu, M.; Li, X.; Liu, L.; Kou, J.; Wang, Y.; et al. Independent and combined effects of exposure to organophosphate esters on thyroid hormones in children and adolescents. *Environ. Geochem. Health* **2023**, *45*, 3833–3846. [[CrossRef](#)]
20. Zhang, Q.; Ji, C.; Yin, X.; Yan, L.; Lu, M.; Zhao, M. Thyroid hormone-disrupting activity and ecological risk assessment of phosphorus-containing flame retardants by in vitro, in vivo and in silico approaches. *Environ. Pollut.* **2016**, *210*, 27–33. [[CrossRef](#)]
21. Zhang, Q.; Lu, M.; Dong, X.; Wang, C.; Zhang, C.; Liu, W.; Zhao, M. Potential Estrogenic Effects of Phosphorus-Containing Flame Retardants. *Environ. Sci. Technol.* **2014**, *48*, 6995–7001. [[CrossRef](#)]
22. Cui, D.; Bi, J.; Zhang, Z.-N.; Li, M.-Y.; Qin, Y.-S.; Xiang, P.; Ma, L.Q. Organophosphorus flame retardant TDCPP-induced cytotoxicity and associated mechanisms in normal human skin keratinocytes. *Sci. Total Environ.* **2020**, *726*, 138526. [[CrossRef](#)]
23. Johnson, C.H.; Patterson, A.D.; Idle, J.R.; Gonzalez, F.J.; Sciences, B. Xenobiotic Metabolomics: Major Impact on the Metabolome. *Annu. Rev. Pharmacol. Toxicol.* **2012**, *52*, 37–56. [[CrossRef](#)]
24. Lipscomb, J.C.; Poet, T.S. In vitro measurements of metabolism for application in pharmacokinetic modeling. *Pharmacol. Ther.* **2008**, *118*, 82–103. [[CrossRef](#)] [[PubMed](#)]

25. Cederbaum, A.I. Molecular mechanisms of the microsomal mixed function oxidases and biological and pathological implications. *Redox Biol.* **2015**, *4*, 60–73. [[CrossRef](#)]
26. Pazzi, G.; Buiarelli, F.; Di Filippo, P.; Pomata, D.; Riccardi, C.; Lucarelli, F.; Giardi, F.; Sonego, E.; Galarini, R.; Lorenzetti, S.; et al. Metals and organic species associated with fine and coarse aerosol particles in an electronic waste recycling plant. *Air Qual. Atmos. Health* **2023**, *16*, 841–856. [[CrossRef](#)]
27. Pomata, D.; Di Filippo, P.; Riccardi, C.; Buiarelli, F.; Marini, F.; Romani, L.; Lucarelli, F.; Pazzi, G.; Galarini, R.; Simonetti, G. Concentrations and co-occurrence of 101 emerging and legacy organic pollutants in the ultrafine, fine and coarse fractions of airborne particulates associated with treatment of waste from electrical and electronic equipment. *Chemosphere* **2023**, *338*, 139443. [[CrossRef](#)] [[PubMed](#)]
28. Pyo, S.M.; Maibach, H.I. Skin Metabolism: Relevance of Skin Enzymes for Rational Drug Design. *Skin Pharmacol. Physiol.* **2019**, *32*, 283–293. [[CrossRef](#)]
29. Van Den Eede, N.; Maho, W.; Erratico, C.; Neels, H.; Covaci, A. First insights in the metabolism of phosphate flame retardants and plasticizers using human liver fractions. *Toxicol. Lett.* **2013**, *223*, 9–15. [[CrossRef](#)]
30. Selmi-Ruby, S.; Marín-Sáez, J.; Fildier, A.; Buleté, A.; Abdallah, M.; Garcia, J.; Deverchère, J.; Spinner, L.; Giroud, B.; Ibanez, S.; et al. In vivo characterisation of the toxicological properties of DPhP, one of the main degradation products of aryl phosphate esters. *Environ. Health Perspect.* **2020**, *128*, 127006. [[CrossRef](#)]
31. Alves, A.; Erratico, C.; Lucattini, L.; Cuykx, M.; Leonards, P.E.G.; Voorspoels, S.; Covaci, A. Mass spectrometric identification of in vitro-generated metabolites of two emerging organophosphate flame retardants: V6 and BDP. *Chemosphere* **2018**, *212*, 1047–1057. [[CrossRef](#)] [[PubMed](#)]
32. Van Den Eede, N.; Erratico, C.; Exarchou, V.; Maho, W.; Neels, H.; Covaci, A. In vitro biotransformation of tris (2-butoxyethyl) phosphate (TBOEP) in human liver and serum. *Toxicol. Appl. Pharmacol.* **2015**, *284*, 246–253. [[CrossRef](#)]
33. Zamora, I.; Fontaine, F.; Serra, B.; Plasencia, G. High-throughput, computer assisted, specific MetID. A revolution for drug discovery. *Drug Discov. Today Technol.* **2013**, *10*, e199–e205. [[CrossRef](#)]
34. Radchenko, T.; Zamora, I.; Fontaine, F.; Moretoni, L.; Design, L.M.; Cugat, S. WebMetabase: Cleavage sites analysis tool for natural and unnatural substrates from diverse data source. *Bioinformatics* **2018**, *35*, 650–655. [[CrossRef](#)] [[PubMed](#)]
35. Goracci, L.; Desantis, J.; Valeri, A.; Castellani, B.; Eleuteri, M.; Cruciani, G. Understanding the Metabolism of Proteolysis Targeting Chimeras (PROTACs): The Next Step toward Pharmaceutical Applications. *J. Med. Chem.* **2020**, *63*, 11615–11638. [[CrossRef](#)] [[PubMed](#)]
36. Rolsted, K.; Kissmeyer, A.; Rist, M.G.; Hansen, S.H. Evaluation of cytochrome P450 activity in vitro, using dermal and hepatic microsomes from four species and two keratinocyte cell lines in culture. *Arch. Dermatol. Res.* **2008**, *300*, 11–18. [[CrossRef](#)]
37. Herczegh, S.M.; Chu, S.; Letcher, R.J. Biotransformation of bisphenol-A bis(diphenyl phosphate): In vitro, in silico, and (non-) target analysis for metabolites in rat and bird liver microsomal models. *Chemosphere* **2023**, *310*, 136796. [[CrossRef](#)]

**Disclaimer/Publisher’s Note:** The statements, opinions and data contained in all publications are solely those of the individual author(s) and contributor(s) and not of MDPI and/or the editor(s). MDPI and/or the editor(s) disclaim responsibility for any injury to people or property resulting from any ideas, methods, instructions or products referred to in the content.